coatings

MDPI

Article

The Improved Non-Polar Gas Sensing Performance of Surface-Modified Porous Silicon-Based Gas Sensors

Bakyt Khaniyev, Margulan Ibraimov, Yerulan Sagidolda *, Yerbolat Tezekbay, Tolagay Duisebayev, Ayan Tileu and Ainur Khaniyeva

Department of Physics and Technology, Al-Farabi Kazakh National University, Almaty 050040, Kazakhstan
* Correspondence: erulan.sagidolda@kaznu.kz

Abstract: The present article studied gas sensor sensing characteristics based on surface-modified porous silicon (PS) by depositing the metal oxide semiconductor layer. The PS layer was prepared through the electrochemical etching of crystalline silicon in an HF-based solution. DC magnetron sputtering technology was used to obtain the p-CuO layer on the surface of the p-PS. The obtained material's structural, morphological, and sensing behavior were investigated using SEM, XRD, Raman spectra, and the current–voltage characteristics. For the detection of toluene and chloroform vapors, a planar structure was used. The sensing response value revealed that the CuO/PS-based gas sensors have good sensitivity for toluene and chloroform vapors. The sensing mechanism is explained using schematic energy band diagrams. Therefore, this approach is helpful for the development of a simple, cost-effective sensor for detecting non-polar chemical analytes.

Keywords: porous silicon; heterostructure; magnetron sputtering; copper oxide; toluene gas sensor; chloroform; sensitivity

check for updates

Citation: Khaniyev, B.; Ibraimov, M.; Sagidolda, Y.; Tezekbay, Y.; Duisebayev, T.; Tileu, A.; Khaniyeva, A. The Improved Non-Polar Gas Sensing Performance of Surface-Modified Porous Silicon-Based Gas Sensors. *Coatings* **2023**, *13*, 190. https://doi.org/10.3390/coatings13010190

Academic Editor: P. Poornesh

Received: 27 December 2022
Revised: 11 January 2023
Accepted: 13 January 2023
Published: 15 January 2023

Copyright: © 2023 by the authors. Licensee MDPI, Basel, Switzerland. This article is an open access article distributed under the terms and conditions of the Creative Commons Attribution (CC BY) license (https://creativecommons.org/licenses/by/4.0/).

1. Introduction

Our environment contains various types of gases that can harm human health. They pollute the atmosphere and contribute to industrial harm and medical conditions [1,2].

Among the various harmful gases, toluene and chloroform are extensively used in pharmaceuticals, laboratory solvents, fuels, paint thinners, and inks [2,3]. Chloroform is a powerful anesthetic, euphoriant, anxiolytic, and sedative when inhaled or ingested [4]. Additionally, toluene vapors at high concentrations have a narcotic effect on a person, causing severe hallucinations [3,5]. Therefore, the fabrication of high-precision toluene gas sensors with high sensitivity, fast response, good selectivity, low limit of detection (LOD), and in situ and real-time monitoring tools is paramount to ensure the safety of healthcare. Nowadays, toluene and chloroform vapors can be detected using various gas sensors including metal oxide, electrochemical, organic compound, optical, and carbon-based gas sensors [2–5].

Most gas sensors are made from metal oxide semiconductors (MOS). P-type MOS, such as NiO [6], Co_3O_4 [7], and CuO [8,9], have their own characteristics. As CuO is one of the most essential p-type semiconductors, a few articles have reported on the sensing performances of CuO nanopowders, nanorods, and nanowires. Wang et al. [10] reported that CuO/WO_3 composites showed great sensing performance at 10 ppm H_2S at 70 °C and excellent selectivity. Bhowmick et al. [11] indicated that CuO/ZnO bilayer thin films exhibited good CO_2 sensing characteristics at 375 °C. Steinhauer et al. [12] reported that CuO nanowires decorated with Pd nanoparticles showed high sensitivity to CO at 350 °C. Gas sensors based only on MOS, currently used in practice, in most cases, work at high temperatures and are also poorly compatible with modern silicon-based electronic devices. They also suffer from low sensitivity, limited selectivity, and slow response. Although these sensors have a high sensitivity to toluene vapors, they usually have a high operating

temperature, which can increase power consumption, and have complex and expensive production technologies [13].

The large surface area of porous silicon (PS), its tendency towards chemical reactions, and other unique optical and electrical properties allow it to be used in various gas sensors at room temperature [14]. Unlike metal oxides, gas sensors based on PS do have good compatibility with current electronic technologies [15]. Manakov et al. [16] used PS material as a sensitive material for a capacitive gas sensor to detect some organic compounds such as acetonitrile and chloroform. However, the PS material is usually unstable; that is, the material's surface is degraded over time under the influence of various factors [17]. Thus, by depositing CuO on the PS surface and creating a heterojunction structure, it is possible to improve its sensing performance at room temperature [18].

Yan et al. reported on the NO_2 gas sensing performance of WO_3/PS heterojunctions at room temperature [19]. Other researchers have studied PS/Cu_2O [20], PS/TeO_2 [21], and PS/V_2O_5 [22]. In such structures, the high surface area provided by PS, together with p–n or p–p heterojunctions, act as a strong source of resistance modulation, which ultimately can enhance their gas-sensing properties.

The main purpose of this work is to investigate the sensing performance of CuO/PS heterostructure as a cost-effective, simple gas sensor for toluene and chloroform vapors.

2. Materials and Methods

The porous silicon (PS) samples used to perform the experiments described in this work were obtained via the electrochemical etching method, as described in our previous work [13,14]. The porous layer was obtained on the surface of a p-type silicon wafer with the orientation <100> and resistance 10 Ohm·cm. Pieces of the silicon wafer with the dimensions 1 × 1 cm^2 were cut for ease of operation. Before starting the etching process, the silicon surface was soaked in HF solution for 10 s and then cleaned with ethanol. The electrochemical etching process was carried out in a fluoroplastic Teflon cell in an electrolyte containing HF and ethanol in a volume ratio of 1:1. The etching current was 5 mA, and the etching time was 40 min. Samples were then washed with deionized water and dried in the air. The porosity was measured with the gravimetric method [23].

Copper oxide (CuO) was deposited on the surface of the PS with the magnetron sputtering method. The magnetron sputtering process was performed on the Kurt J. Lesker LAB-18 magnetron system (Kurt J. Lesker Company, Dresden, Germany). A CuO target with a purity of 99.999% was used. The distance between the target and the sample was 13 cm. The initial vacuum pressure was 5 × 10^{-6} Torr, and the working pressure was 10.5 mTorr. In addition, Ar and O_2 gases were introduced into the magnetron sputtering system, with flow rates of 40 sccm and 10 sccm, respectively. The deposition power was 100 W and the deposition time was 30 min. After the formation of CuO on the surface of the PS sample, the sample was kept in a furnace at a temperature of 650 °C for 4 h in order to crystallize. The thickness of the CuO on the surface of the PS was determined using a profilometer Dektak XT Stylus profilometer (Bruker, Billerica, Massachusetts, USA).

The morphology of the samples was studied using a scanning electron microscope JSM-IT2000 (JEOL Ltd., Tokyo, Japan). The XRD spectra used to study the phase formation of the samples were obtained on a Rigaku Miniflex 600 diffractometer (Rigaku, Tokyo, Japan). Moreover, the reflectance spectra of the samples were measured on a Shimadzu UV-3600 spectrophotometer (Shimadzu, Kyoto, Japan) in the wavelength range of 240–830 nm. Two ohmic contacts of InGa alloy in the coplanar configuration were deposited on the samples' surface by thermal installation to obtain electrical characteristics. The sensitivity of the samples to toluene and chloroform vapors was calculated as in [13].

3. Results and Discussion

The porosity of the PS substrate amounted to 72.7%. The thickness of the CuO layer defined by the profilometer was 130 nm.

The surface morphologies of the PS and the CuO/PS samples are shown in Figure 1. From Figure 1, it is clearly observed that the PS surface is porous in nature and pore-like structures are spread throughout the surface. Figure 1b displays the surface of CuO deposited on PS, and it can be seen that it also has a uniform porous structure.

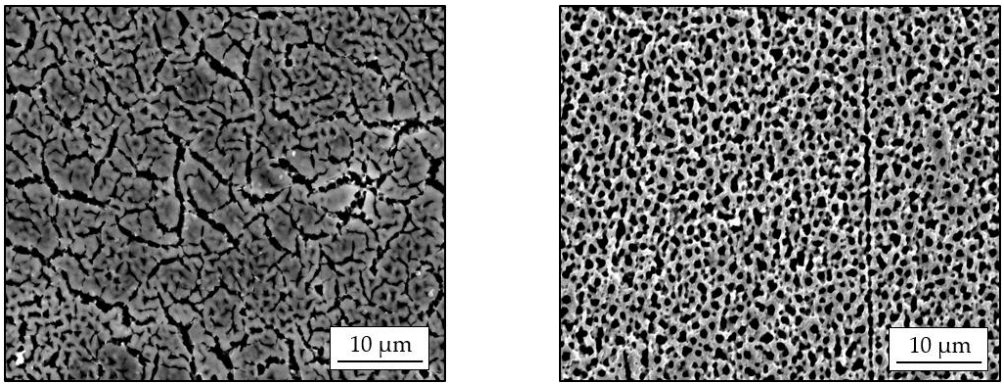


Figure 1. SEM images of samples: (**a**) PS; (**b**) CuO/PS.

Figure 2a shows the XRD pattern recorded in the 10–90° 2θ range to verify the crystal structures of the PS and CuO/PS. A sharp diffraction peak can be seen at 69.2° for the as-prepared PS sample, corresponding to the plane reflection of Si [24]. Additionally, there is a broad hump in the region of 15–30° and it is likely related to the formation of an amorphous SiO_2 phase [25]. The strong diffraction peaks of CuO appear at 35.662°, 38.853°, and 48.954° in the red pattern in Figure 2. They correspond to <−1 1 1>, <1 1 1>, and <2 0 0> planes, respectively [26]. The peaks of the PS still exist because CuO does not entirely cover the surface of the PS. The values match precisely with the standard data (PDF Card No.: 00-041-0254).

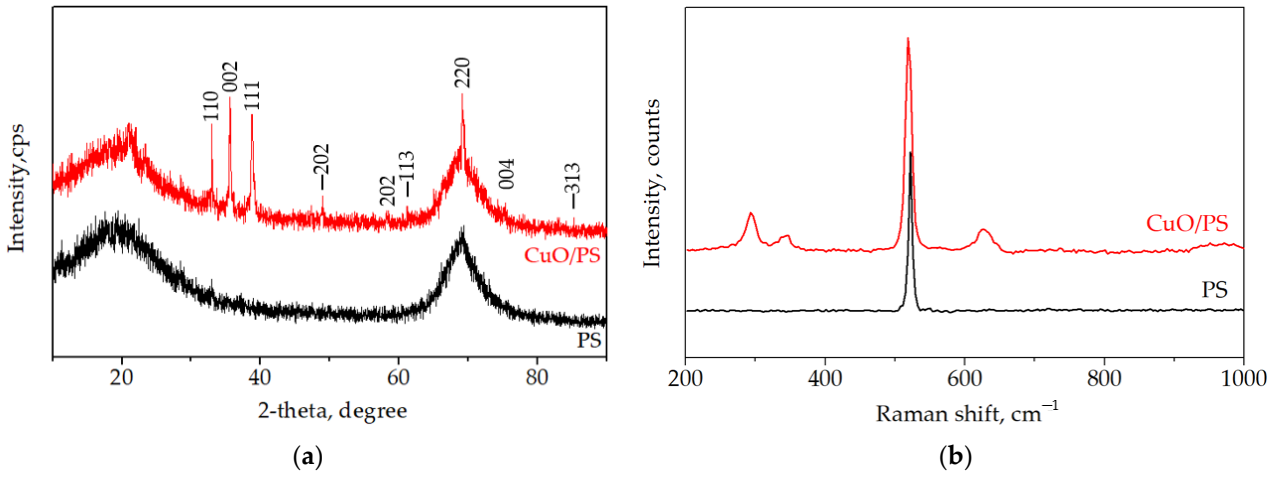


Figure 2. XRD (**a**) and Raman (**b**) spectra of PS and CuO/PS.

Figure 2b shows Raman spectra of the PS sample and CuO/PS heterostructure material.

It can be noted that the Raman spectra of the samples exhibit peak intensity at 520 cm^{-1}. It is described as first-order scattering on the phonon in the middle of the Brillouin zone (Γ), obeying the selection rule $|k| \approx 0$. The frequency of the Raman band corresponds to the frequency of phonons in Γ, which is 15.56 THz (520.7 cm^{-1}) [27]. In summary, this is the main combination scattering band that occurs from the action of

monochromatic light with a crystal lattice of PS. Raman analysis of CuO revealed peaks at 296 cm^{-1}, 346 cm^{-1}, and 631 cm^{-1}, which are widespread in this material [28].

The current–voltage characteristics of the samples were measured at a constant concentration of toluene and chloroform gas at room temperature using the special sealed box and NI Elvis II+ module. The desired gas concentration in the sealed box is determined by the formula (2) in [13]. It can be seen from Figure 3 that the current strength of the sample changes under the influence of ethanol, ammonia, toluene, and chloroform vapors.

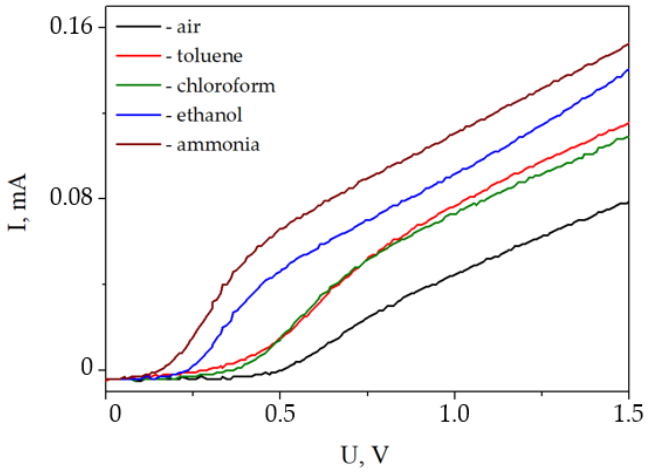


Figure 3. The current–voltage characteristics of CuO/PS-based gas sensor in the presence of various gas types.

Figure 4 shows sensitivity diagrams of gas sensors based on PS and CuO/PS to ammonia, ethanol, toluene, and chloroform vapors. It can be seen that the PS-based gas sensor has good sensitivity to ammonia vapor, but it cannot be used to detect non-polar gases such as toluene and chloroform. From Figure 4b, it is clear that the CuO/PS heterostructure-based gas sensor has a sensitivity value of up to 33.9 to toluene vapor and 27.6 to chloroform vapor. The CuO/PS gas sensor exhibited the response and recovery time of 50 s and 60 s, respectively, to 0.1 ppm toluene and chloroform vapors at room temperature.

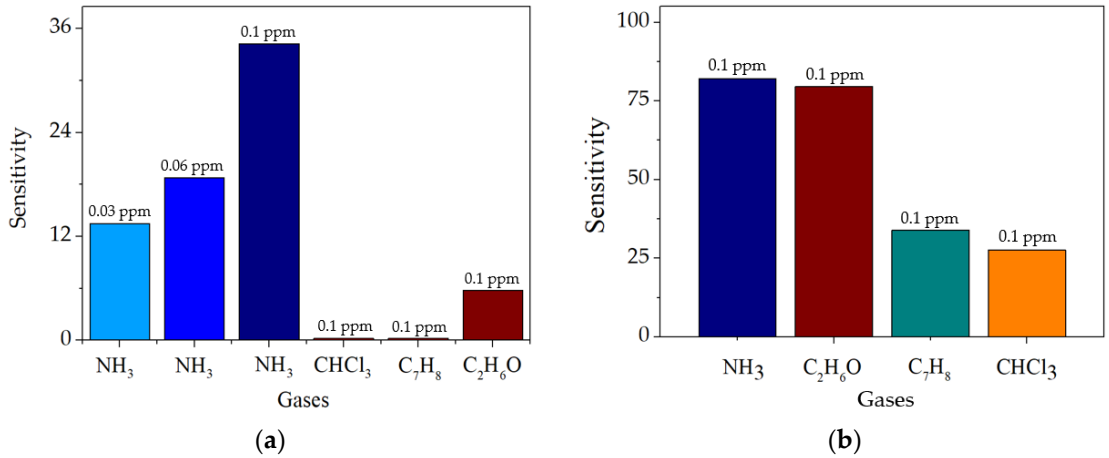


Figure 4. Sensitivity diagrams of gas sensors based on PS (**a**) and CuO/PS (**b**) to different gas types.

Figure 5 shows the dynamic response curves of the sensor to 0.1 ppm toluene and chloroform vapors measured at constant voltage U = 2 V. Table 1 compares the sensing characteristics of the CuO/PS sensor to toluene and chloroform vapors with other metal oxide-based gas sensors.

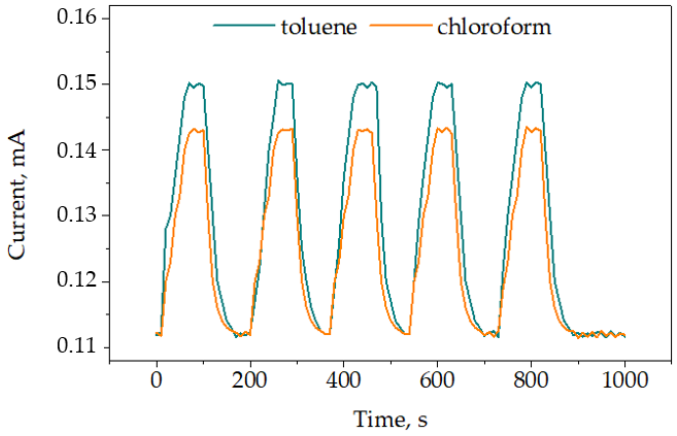


Figure 5. Dynamic response curves of the sensor to 0.1 ppm toluene and chloroform vapors.

Table 1. Comparison of toluene and chloroform gas sensors.

Sensing Material	Target Gas	Sensitivity	Working Temperature, °C	Concentration, ppm	Reference
$(C_3N_4)_{0.12}Co_3O_4$	Toluene	17.02	220	100	[29]
Ag/Bi_2O_3	Toluene	89.2	26	50	[2]
$Ag_{0.4}Pd_{0.6}@In_2O_3$	Toluene	15.9	180	1	[30]
rGO-MWCNT (5 mg)- α-Fe_2O_3	Chloroform	16	26	1	[4]
RGO	Chloroform	4.3	26	800	[31]
CuO/PS	Toluene Chloroform	33.9 27.6	26	0.1	This work

The energy band diagram shown in Figure 6 can be used to understand the gas sensing mechanism of the CuO/PS semiconductor heterostructure. The bandgap energy (E_g) of PS is greater than that of crystalline silicon (1.12 eV) due to the quantum size effect. The electron affinity of PS is close to that of silicon (χ = 4.01 eV) [26,32]. For p-type CuO material, these values are E_g = 1.35 eV, χ = 4.07 eV [26]. When PS and CuO bond together, a p-p heterostructure is formed, as shown in Figure 6.

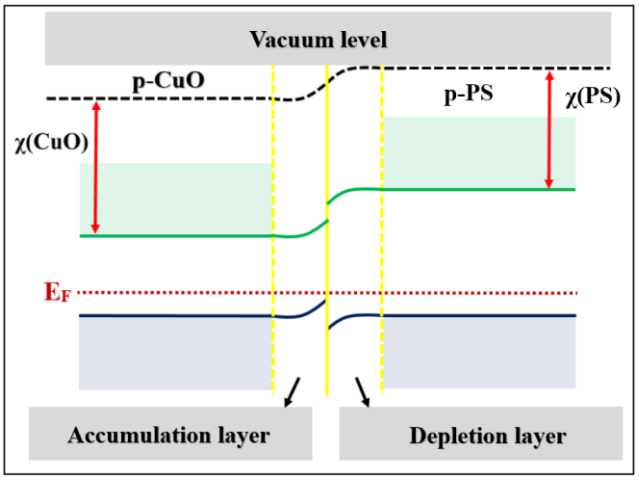


Figure 6. Energy band diagram of the CuO/PS [26].

Since the Fermi energies are not on the same level, the CuO electrons move towards the PS, and the holes move in the opposite direction until the Fermi energies are equal. This leads to the formation of a depletion layer of holes on the PS side, and an accumulation layer of holes on the CuO side [26].Due to the different dielectric constants of CuO and PS, the bending energy bands near the junction in the energy band diagram are broken. The effective separation of charges provides a high concentration of charge carriers in the accumulation layer. Therefore, the exchange of electrons with the adsorbed gas is easy [33]. When the sensor is in the air, oxygen is adsorbed on the material's surface. Due to the large surface area of the material, it can provide many active centers for adsorbing gas molecules. The higher the specific surface area, the higher the number of oxygen vacancies on the material's surface. Thus, the sensor adsorbs many oxygen molecules at room temperature. Oxygen molecules adsorbed on the surface exchange with electrons on the sensor surface to form oxygen ions O_2^- which are stable at the working room temperature [34].

$$O_2 \rightarrow O_2\ (ads)$$

$$O_2 + e^- \rightarrow O_2^-\ (ads)$$

As a result, the energy band of the CuO/PS heterojunction is further bent. When gas molecules affect the sensor, an acidification reaction takes place between gas molecules and oxygen anions, the concentration of defects in the accumulation layer increases, and the material resistance decreases [35].

The chemical reactions of ammonia, ethanol, toluene, and chloroform gas molecules with O_2^- oxygen ions on the CuO/PS surface can be written by the following expressions [2,36–38]:

$$4NH_3 + 5O_2^-\ (ads) \rightarrow 4NO + 6H_2O + 5e^-$$

$$C_2H_6O + 3O_2^-\ (ads) \rightarrow 3H_2O + 2CO_2 + 3e^-$$

$$C_7H_8 + 9O_2^-\ (ads) \rightarrow 4H_2O + 7CO_2 + 9e^-$$

$$2CHCl_3 + O_2^-\ (ads) \rightarrow 2COCl_2 + HCl + e^-$$

Accordingly, more electrons are extracted from the surface of the sensor, and the resistance of the CuO/PS sensor decreases. In fact, due to an increase in the width of the hole in the accumulation layer, more holes participate in the material's conductivity, and the conductivity increases. When the concentration of gases increases, more electrons can be extracted by gases, and a higher response can be observed.

4. Conclusions

To summarize, this work demonstrates the sensing performance of the CuO/PS heterojunction structure obtained by the DC magnetron sputtering method on the PS surface for toluene and chloroform vapors. The structure and morphology of the etched and sputtered nanomaterials were studied using XRD, Raman spectra, and SEM analysis; they confirmed the deposition of CuO on the PS surface. From the gas sensing results, CuO/PS demonstrated a better toluene and chloroform response at room temperature than PS. Therefore, the modification of the PS surface with the CuO layer led to the enhancement of their sensitivity to vapors. This study shows that it is possible to fabricate a highly sensitive, inexpensive gas sensor device based on CuO/PS heterostructure for determining toluene and chloroform vapors in concentrations up to 0.1 ppm at room temperature. However, it is obvious that many studies are needed prior to the application of this material as a toluene and chloroform sensor.

Author Contributions: Conceptualization, B.K., M.I., and Y.S.; methodology, B.K., Y.S., and A.T.; validation, M.I., A.K., and B.K.; investigation, B.K., A.T., Y.T., and T.D.; resources, A.K. and T.D.; data curation, B.K. and A.K.; writing—original draft preparation, B.K.; writing—review and editing, M.I. and T.D.; supervision, M.I. and Y.S.; All authors have read and agreed to the published version of the manuscript.

Funding: This research was funded by the Ministry of Education and Science of the Republic of Kazakhstan, grant number: AP13268784.

Institutional Review Board Statement: Not applicable.

Informed Consent Statement: Not applicable.

Data Availability Statement: Not applicable.

Conflicts of Interest: The authors declare no conflict of interest.

References

1. Dong, C.; Zhao, R.; Yao, L.; Ran, Y.; Zhang, X.; Wang, Y. A review on WO_3 based gas sensors: Morphology control and enhanced sensing properties. *J. Alloys Compd.* **2020**, *820*, 153194. [CrossRef]
2. David, S.S.; Veeralakshmi, S.; Sandhya, J.; Nehru, S.; Kalaiselvam, S. Room temperature operatable high sensitive toluene gas sensor using chemiresistive Ag/Bi_2O_3 nanocomposite. *Sens. Actuators B Chem.* **2020**, *320*, 128410. [CrossRef]
3. Mokoena, T.P.; Swart, H.C.; Hillie, K.T.; Motaung, D.E. Engineering of rare-earth Eu^{3+} ions doping on p-type NiO for selective detection of toluene gas sensing and luminescence properties. *Sens. Actuators B Chem.* **2021**, *347*, 130530. [CrossRef]
4. Basu, A.K.; Sah, A.N.; Dubey, M.M.; Dwivedi, P.K.; Pradhan, A.; Bhattacharya, S. MWCNT and α-Fe_2O_3 embedded rGO-nanosheets based hybrid structure for room temperature chloroform detection using fast response/recovery cantilever based sensors. *Sens. Actuators B Chem.* **2020**, *305*, 127457. [CrossRef]
5. Karuppasamy, K.; Sharma, B.; Vikraman, D.; Jo, E.B.; Sivakumar, P.; Kim, H.S. Switchable pn gas response for 3D-hierarchical $NiFe_2O_4$ porous microspheres for highly selective and sensitive toluene gas sensors. *J. Alloys Compd.* **2021**, *886*, 161281. [CrossRef]
6. Li, C.; Choi, P.G.; Kim, K.; Masuda, Y. High Performance Acetone Gas Sensor Based on Ultrathin Porous NiO Nanosheet. *Sens. Actuators B Chem.* **2022**, *367*, 132143. [CrossRef]
7. Cheng, P.; Dang, F.; Wang, Y.; Gao, J.; Xu, L.; Wang, C.; Lv, L.; Li, X.; Zhang, B.; Liu, B. Gas sensor towards n-butanol at low temperature detection: Hierarchical flower-like Ni-doped Co_3O_4 based on solvent-dependent synthesis. *Sens. Actuators B Chem.* **2021**, *328*, 129028. [CrossRef]
8. Wang, N.; Tao, W.; Gong, X.; Zhao, L.; Wang, T.; Zhao, L.; Liu, F.; Liu, X.; Sun, P.; Lu, G. Highly sensitive and selective NO_2 gas sensor fabricated from Cu_2O-CuO microflowers. *Sens. Actuators B Chem.* **2022**, *362*, 131803. [CrossRef]
9. Khot, S.; Phalake, S.; Mahadik, S.; Baragale, M.; Jagadale, S.; Burungale, V.; Navale, Y.; Patil, V.; Patil, V.; Patil, P.; et al. Synthesis of CuO thin film sensors by spray pyrolysis method for NO_2 gas detection. *Mater. Today Proc.* **2021**, *43*, 2694–2697. [CrossRef]
10. Wang, Y.; Zhang, S.; Xiao, D.; Wang, S.; Zhang, T.; Yang, X.; Heng, S.; Sun, M. CuO/WO_3 hollow microsphere PN heterojunction sensor for continuous cycle detection of H_2S gas. *Sens. Actuators B Chem.* **2023**, *374*, 132823. [CrossRef]
11. Bhowmick, T.; Ghosh, A.; Nag, S.; Majumder, S.B. Sensitive and selective CO_2 gas sensor based on CuO/ZnO bilayer thin-film architecture. *J. Alloys Compd.* **2022**, *903*, 163871. [CrossRef]
12. Steinhauer, S.; Singh, V.; Cassidy, C.; Gspan, C.; Grogger, W.; Sowwan, M.; Köck, A. Single CuO nanowires decorated with size-selected Pd nanoparticles for CO sensing in humid atmosphere. *Nanotechnology* **2015**, *26*, 175502. [CrossRef] [PubMed]
13. Khaniyev, B.A.; Sagidolda, Y.; Dikhanbayev, K.K.; Tileu, A.O.; Ibraimov, M.K. High sensitive NH_3 sensor based on electrochemically etched porous silicon. *Cogent Eng.* **2020**, *7*, 1810880. [CrossRef]
14. Ibraimov, M.K.; Sagidolda, Y.; Rumyantsev, S.L.; Zhanabaev, Z.Z.; Shur, M.S. Selective gas sensor using porous silicon. *Sens. Lett.* **2016**, *14*, 588–591. [CrossRef]
15. Kwon, Y.J.; Mirzaei, A.; Na, H.G.; Kang, S.Y.; Choi, M.S.; Bang, J.H.; Oum, W.; Kim, S.S.; Kim, H.W. Porous Si nanowires for highly selective room-temperature NO_2 gas sensing. *Nanotechnology* **2018**, *29*, 294001. [CrossRef] [PubMed]
16. Manakov, S.M.; Ibraimov, M.K.; Sagidolda, Y.; Zhumatova, S.A.; Darmenkulova, M.B. Detection of acetonitrile and chloroform using structures on the base of porous silicon. *Eurasian Chem.-Technol. J.* **2019**, *21*, 89–93. [CrossRef]
17. Wu, Y.; Hu, M.; Qin, Y.; Wei, X.; Ma, S.; Yan, D. Enhanced response characteristics of p-porous silicon (substrate)/p-TeO_2 (nanowires) sensor for NO_2 detection. *Sens. Actuators B Chem.* **2014**, *195*, 181–188. [CrossRef]
18. Bang, J.H.; Choi, M.S.; Mirzaei, A.; Oum, W.; Han, S.; Kim, S.S.; Kim, H.W. Porous Si/SnO_2 nanowires heterostructures for H_2S gas sensing. *Ceram. Int.* **2020**, *46*, 604–611. [CrossRef]
19. Yan, D.; Li, S.; Liu, S.; Tan, M.; Cao, M. Electrodeposited tungsten oxide films onto porous silicon for NO_2 detection at room temperature. *J. Alloys Compd.* **2018**, *735*, 718–727. [CrossRef]
20. Yan, D.; Li, S.; Hu, M.; Liu, S.; Zhu, Y.; Cao, M. Electrochemical synthesis and the gas-sensing properties of the Cu_2O nanofilms/porous silicon hybrid structure. *Sens. Actuators B Chem.* **2016**, *223*, 626–633. [CrossRef]

21. Bang, J.H.; Choi, M.S.; Mirzaei, A.; Han, S.; Lee, H.Y.; Choi, S.W.; Kim, S.S.; Kim, H.W. Hybridization of silicon nanowires with TeO_2 branch structures and Pt nanoparticles for highly sensitive and selective toluene sensing. *Appl. Surf. Sci.* **2020**, *525*, 146620. [CrossRef]
22. Qiang, X.; Hu, M.; Zhou, L.; Liang, J. Pd nanoparticles incorporated porous silicon/V_2O_5 nanopillars and their enhanced p-type NO_2-sensing properties at room temperature. *Mater. Lett.* **2018**, *231*, 194–197. [CrossRef]
23. Harraz, F.A. Porous silicon chemical sensors and biosensors: A review. *Sens. Actuators B Chem.* **2014**, *202*, 897–912. [CrossRef]
24. Harraz, F.A.; Ismail, A.A.; Al-Sayari, S.A.; Al-Hajry, A.; Al-Assiri, M.S. A highly sensitive and durable electrical sensor for liquid ethanol using thermally-oxidized mesoporous silicon. *Superlattices Microstruct.* **2016**, *100*, 1064–1072. [CrossRef]
25. Salem, A.M.S.; Harraz, F.A.; El-Sheikh, S.M.; Hafez, H.S.; Ibrahim, I.A.; Abdel-Mottaleb, M.S.A. Enhanced electrical and luminescent performance of a porous silicon/MEH-PPV nanohybrid synthesized by anodization and repeated spin coating. *RSC Adv.* **2015**, *5*, 99892–99898. [CrossRef]
26. Liu, X.; Hu, M.; Wang, Y.; Liu, J.; Qin, Y. High sensitivity NO_2 sensor based on CuO/p-porous silicon heterojunction at room temperature. *J. Alloys Compd.* **2016**, *685*, 364–369. [CrossRef]
27. Kadlečíková, M.; Breza, J.; Vančo, Ľ.; Mikolášek, M.; Hubeňák, M.; Racko, J.; Greguš, J. Raman spectroscopy of porous silicon substrates. *Optik* **2018**, *174*, 347–353. [CrossRef]
28. Tran, T.H.; Nguyen, V.T. Copper oxide nanomaterials prepared by solution methods, some properties, and potential applications: A brief review. *Int. Sch. Res. Not.* **2014**, *14*, 856592. [CrossRef] [PubMed]
29. Niu, J.Y.; Wang, L.; Xu, J.C.; Jin, H.X.; Hong, B.; Jin, D.F.; Peng, H.L.; Wang, X.Q. Mesoporous Co_3O_4 nanowires decorated with g-C_3N_4 nanosheets for high performance toluene gas sensors based on pn heterojunction. *Mater. Chem. Phys.* **2023**, *293*, 126980. [CrossRef]
30. Liu, X.; Duan, X.; Zhang, C.; Hou, P.; Xu, X. Improvement toluene detection of gas sensors based on flower-like porous indium oxide nanosheets. *J. Alloys Compd.* **2022**, *897*, 163222. [CrossRef]
31. Midya, A.; Mukherjee, S.; Roy, S.; Santra, S.; Manna, N.; Ray, S.K. Selective chloroform sensor using thiol functionalized reduced graphene oxide at room temperature, *Mater. Res. Express* **2018**, *5*, 025604. [CrossRef]
32. Yan, D.; Xia, S.; Li, S.; Wang, S.; Tan, M.; Liu, S. Electrophoretic deposition of multiwalled carbon nanotubes onto porous silicon with enhanced NO_2-sensing characteristics. *Mater. Res. Bull.* **2021**, *134*, 111109. [CrossRef]
33. Mashock, M.; Yu, K.; Cui, S.; Mao, S.; Lu, G.; Chen, J. Modulating gas sensing properties of CuO nanowires through creation of discrete nanosized p–n junctions on their surfaces. *ACS Appl. Mater. Interfaces* **2012**, *4*, 4192–4199. [CrossRef] [PubMed]
34. Jaiswal, J.; Singh, P.; Chandra, R. Low-temperature highly selective and sensitive NO_2 gas sensors using CdTe-functionalized ZnO filled porous Si hybrid hierarchical nanostructured thin films. *Sens. Actuators B Chem.* **2021**, *327*, 128862. [CrossRef]
35. Kim, H.J.; Lee, J.H. Highly sensitive and selective gas sensors using p-type oxide semiconductors: Overview. *Sens. Actuators B Chem.* **2014**, *192*, 607–627. [CrossRef]
36. Qiang, X.; Hu, M.; Zhao, B.; Qin, Y.; Zhang, T.; Zhou, L.; Liang, J. Preparation of porous silicon/Pd-loaded WO_3 nanowires for enhancement of ammonia sensing properties at room temperature. *Mater. Sci. Semicond. Process.* **2018**, *79*, 113–118. [CrossRef]
37. Aleksanyan, M.; Sayunts, A.; Shahkhatuni, G.; Simonyan, Z.; Shahnazaryan, G.; Aroutiounian, V. Gas Sensor Based on ZnO Nanostructured Film for the Detection of Ethanol Vapor. *Chemosensors* **2022**, *10*, 245. [CrossRef]
38. Perillo, P.M.; Rodriguez, D.F. A room temperature chloroform sensor using TiO_2 nanotubes. *Sens. Actuators B Chem.* **2014**, *193*, 263–266. [CrossRef]

Disclaimer/Publisher's Note: The statements, opinions and data contained in all publications are solely those of the individual author(s) and contributor(s) and not of MDPI and/or the editor(s). MDPI and/or the editor(s) disclaim responsibility for any injury to people or property resulting from any ideas, methods, instructions or products referred to in the content.